Improving the Resolution of Low Earth Orbit Objects by Multi-Exposure Imaging and Deconvolution

Vishnu Anand Muruganandan
Department of Electrical & Computer Engineering, University of Canterbury, New Zealand
Andrew Lambert
School of Electrical and Information Technology, UNSW, Canberra, Australia
Richard Clare, Steve Weddell
Department of Electrical & Computer Engineering, University of Canterbury, New Zealand

ABSTRACT

Low Earth Orbit satellites imaged through ground-based telescopes are unresolved due to the relative motion of the satellite and atmospheric turbulence. Conventional wavefront sensors combined with tip-tilt mirror and deformable mirror system improve the resolution of satellite images in real time but such a system is relatively expensive and intricate to implement on sky. This paper describes an alternative method, which partially deconvolves satellite images using an estimated Point Spread Function of a closely separated background star in post-processing. In this method, two cameras are placed on-axis of the telescope, synchronized and triggered simultaneously. The first camera has a long exposure to image the faint background stars and a second camera has a short exposure to image fast moving satellites. In post-processing the Lucy-Richardson algorithm is applied to partially restore the blurred image of two derelict satellites (ALOS-1 & SEASAT) and spatial metrics for such extended objects are used to quantify the quality of the restored image.
.

1. INTRODUCTION

Two derelict satellites (ALOS-1 and SEASAT) have been imaged using synchronised dual camera with different exposure times and resulting blurred images were partially resolved by post-processing using the Lucy-Richardson algorithm. The spatial properties of the satellites are estimated for both raw and restored images [1,2]. The authors have tested various deconvolution algorithms on sky and identified the Lucy-Richardson algorithm as having higher accuracy using the metrics to measure the accuracy of an extended object [2,3]. Advanced Land Observing Satellite (ALOS-1) was launched into Low Earth Orbit in 2006 and it became non-functional after five years [4]. Seafaring satellite (SEASAT) was launched into LEO in 1978 and it became non-functional after 110 days of operation [5].

In section 2 operation of the optical telescope, detector, and observation methods are described. In section 3 the deconvolution process is described and an estimate of the length and width of satellites (ALOS-1,and SEASAT) are provided and compared with true length and width of the satellites. In section 4 the results and future work are discussed.

2. BACKGROUND

The Boller and Chivens (B&C) telescope at the University of Canterbury Mount John Observatory (UCMJO) is used for imaging artificial satellites at LEO. The primary aperture and focal length of the B&C are 0.61 m and 3.85 m respectively, and the detector (FLIR GS3) has a sensor width of 11.3mm supporting a pixel width of 5.5μm. Within a Field of View (FoV) of 10 arcminutes, the target is captured over 10 to 20 frames based on the range of the satellite. The telescope is operated at sidereal rate and pointed to a reference star that has expected close proximity to the trajectory of the satellite, and during the estimated time of contact, multiple frames of the satellite with a reference star are imaged. Then the above process is repeated by slewing the telescope to the next reference star, which is in close proximity to the satellite's trajectory.

The number of stars in the sky increases exponentially as the visible magnitude increases, which means the probability of detecting a star is higher with long exposure time. However, due to relative motion of the satellite, a short exposure time is required to image the satellite without motion blur. Hence, we implement a dual camera system with different exposure time to image both satellite and star simultaneously. In the Fig.1 the camera with long exposure of 10 - 20 ms is used to image the faint background stars with a visible magnitude of 6 or less (brighter). The second camera with short exposure of 0.3 – 0.4 ms is used to image the satellites without motion blur. The light from the telescope is proportioned for each camera using a beam splitter, and re-focused on the image plane of both long and short exposure cameras. Both cameras are triggered simultaneously and synchronised during the observation.

The spatial resolution or sampling distance (SD) of a pixel is estimated using Eq.1, where P is the width of the pixel, R is the slanting distance between satellite and telescope, F is focal length of the telescope, V is the orbital velocity of the satellite. The estimate of the required exposure time (ET) to image the satellite without motion blur is made using Eq.2

$$SD = \frac{P \times R}{F} \qquad (1)$$

$$ET = \frac{P}{F} \times \frac{R}{V} \qquad (2)$$

Two factors are considered significant in contributing to the blurring of the image. These are motion blur and distortion due to atmospheric turbulence. The motion blur is avoided by using short exposure time estimated by Eq.2. The PSF of the background star imaged by a longer exposure camera resembles the PSF of the atmosphere and the length of the long exposure (10 - 20 ms) is set to acquire sufficient signals from the stars present but not too long to be destroyed by the evolution of turbulence causing seeing. The Lucy-Richardson algorithm is an iterative process used to partially restore the blurred image of a satellite by an estimated PSF, and by converging to the maximum likelihood solution [2]. Typically, image metrics are based on stars, which are symmetrical point-sources at infinite distances. The image metrics for unsymmetrical and extended satellites are developed to measure the quality of the raw image and deblurred image [3].

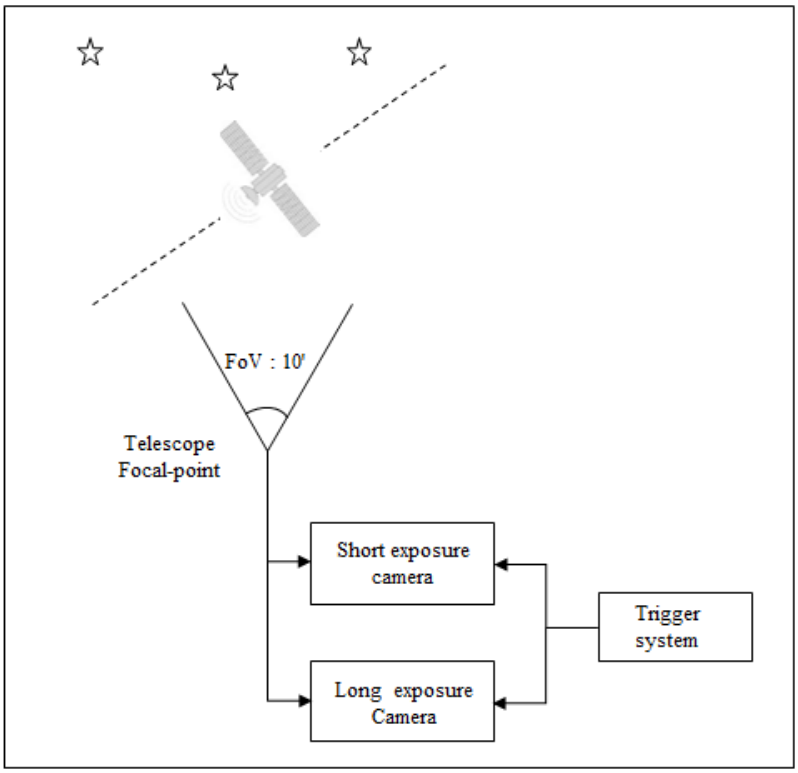

Fig.1: Schematic of multi-exposure imaging to deblur the image of satellites in LEO.

3. Metrics for Extended images and Deconvolution

A local threshold is estimated by averaging the pixel values in the region, and pixels with intensity above the mean value are extracted from the raw image. The extracted pixels are grouped using the nearest neighbour search and if the size (number of pixels) of the group is between 20 to 500 then it is identified as a satellite. The size of the group varies based on the size of the satellite. The "regionprops" function in Matlab is applied to measure the "MajorAxis" (Length) and "MinorAxis" (width) of the satellite in pixels [6]. Subsequently, the estimated length and width of the satellite is converted from pixels to meters, using Eq.1. The estimated length and width of the satellite can then be compared with the true length and width of the satellite to measure the quality of deconvolution.

A star is considered a point-source, object at the image plane that has been perturbed by the Earth's atmosphere, where the spread of the background star represents the PSF estimate for deconvolution. Since the atmosphere condition changes during the observation, a new PSF estimate is used for every image. The isoplanatic angle ($\theta_o < 5$ arcseconds) is an angular limit that separates two point-source objects, where if independent measurements of wavefront perturbations were obtained from each source, the wavefront distortion would be considered equivalent. As the angular separation between reference star and target increases, the wavefront error increases and it is known as angular anisoplanatism [7]. In our observation, the shortest angular distance between the satellite and star is 41 arcseconds, hence the PSF of the star used to deconvolve the images are spatially variant. The "deconvlucy" function in Matlab is used to deblur the satellite image, the size of the star used in PSF estimation is 25x25 pixels and number of iteration to obtain maximum possible solution is 35 [6].

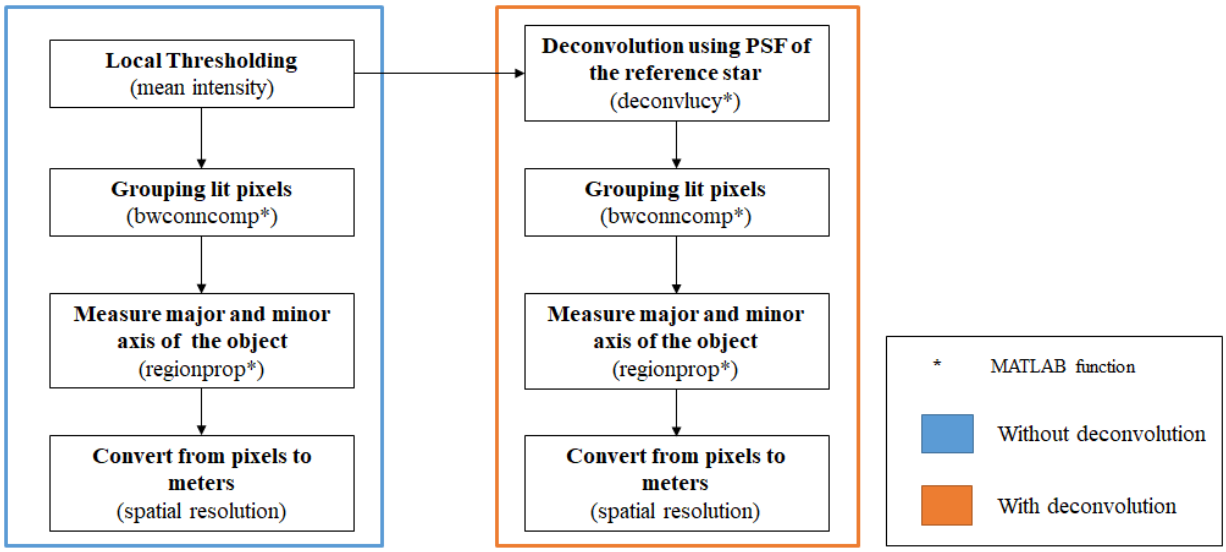

Fig.2: Satellite image processing algorithm with and without deconvolution.

3.1 ALOS

The ALOS in Fig.3 was imaged on 1st November 2020. During the observation the visible magnitude of ALOS is 2.9, elevation is 35 degrees, slanting distance (R) is 1114 km, and required exposure time to image and minimize the satellite motion blur is 0.43 ms, which is shown in Fig.3(b) as stacked images by short exposure camera. The telescope is pointed to the star (HIP54718) shown in a yellow circle in Fig.3(a) as stacked images by long exposure camera. The visible magnitude of the star HIP54718 is 6.3 and exposure time of 10 ms is used to image the star. When the satellite enters the FoV with the star at the center, the trigger system is activated to capture frames for both camera simultaneously. In total, 20 frames are captured within the FoV and 6 frames on either side closest to the star are processed.

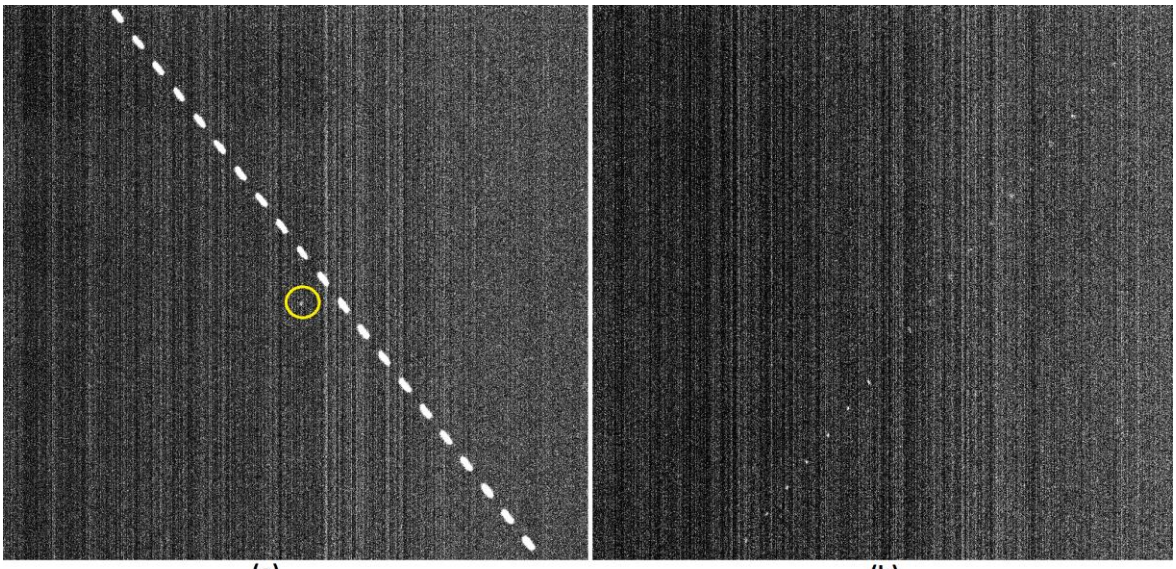

Fig.3: (a) Stacked long exposure images of ALOS and star (HIP54718); (b) Stacked short exposure images of ALOS.

Fig.4(a) shows the CAD model of ALOS, Fig.4(b) is the raw image of ALOS without deconvolution and Fig.4(c) is the deblurred image of ALOS after applying the Lucy-Richardson algorithm. Fig.4 (b & c) are the short exposure image of frame 9. The local mean value (intensity) of the image is 13 (8 bit) and pixels above the mean value are extracted, grouped and identified as a satellite, which is shown in Fig.4(b). The true length and width of ALOS is 27.4 and 9 m respectively [8] and the estimated length and width of the image in Fig.4(b) is 64m and 54.4 m, respectively. The estimated length and width of the image after deconvolution in Fig.4(c) is 27.2 and 14.4m respectively, which are in close proximity to the true length and width of ALOS.

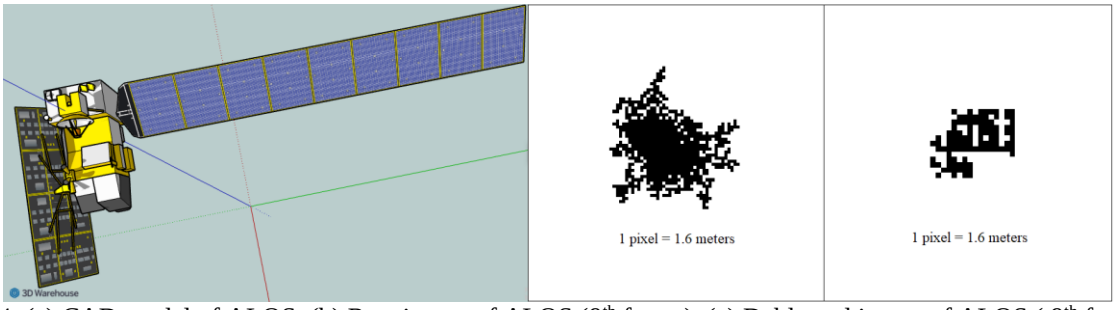

Fig.4: (a) CAD model of ALOS, (b) Raw image of ALOS (9th frame), (c) Deblurred image of ALOS (9th frame).

Fig.5 shows the estimated length of the ALOS with and without deconvolution. The raw image of ALOS shown in Fig.4(b) looks like a blob and it doesn't reveal any physical structure of the satellite because the raw image has been blurred by the atmospheric turbulence. As a result, the estimation of length of ALOS in the raw image (without deconvolution) differs largely from the true length (27.4m) which is shown in Fig.5. However, after deconvolution the blurred image has been partially restored, as show in Fig.4(c), and subsequently, the estimated length with deconvolution corresponds with the true length of ALOS in Fig.5.

Six frames on either side closest to the star are processed in Fig.5. The shortest distance between the ALOS and the reference star is 137 pixels in frame 6 and the corresponding angular distance is 41 arcseconds (0.68 arcminutes). The estimated length with deconvolution is shown to correspond with the true length for frames 7 and 9 but varies moderately in the rest of the frames. Due to angular anisoplanatism, the trend line (cubic) in Fig.5 implies that the accuracy of deconvolution is higher when the satellite is closer to the star, which is around frame 6, and the accuracy decreases when the satellite is further away from the star. Fig.(6), shows the estimated width of the satellite with and without deconvolution. The frames 5 and 7 corresponds with true width (9 m) and rest of the frames varies moderately from true width.

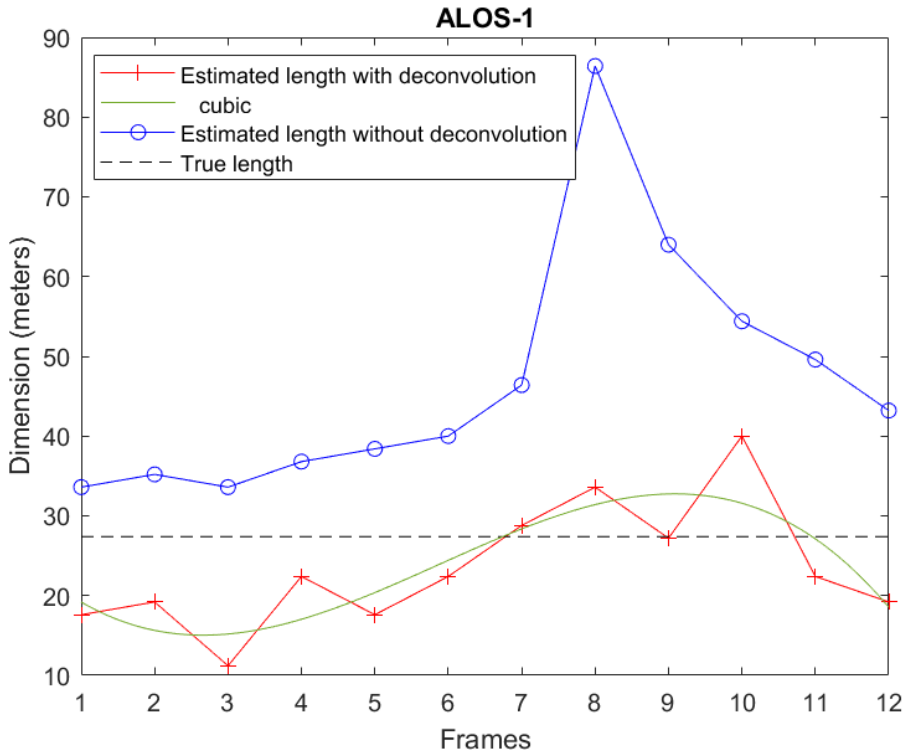

Fig.5: The estimated length of raw and deblurred images of ALOS.

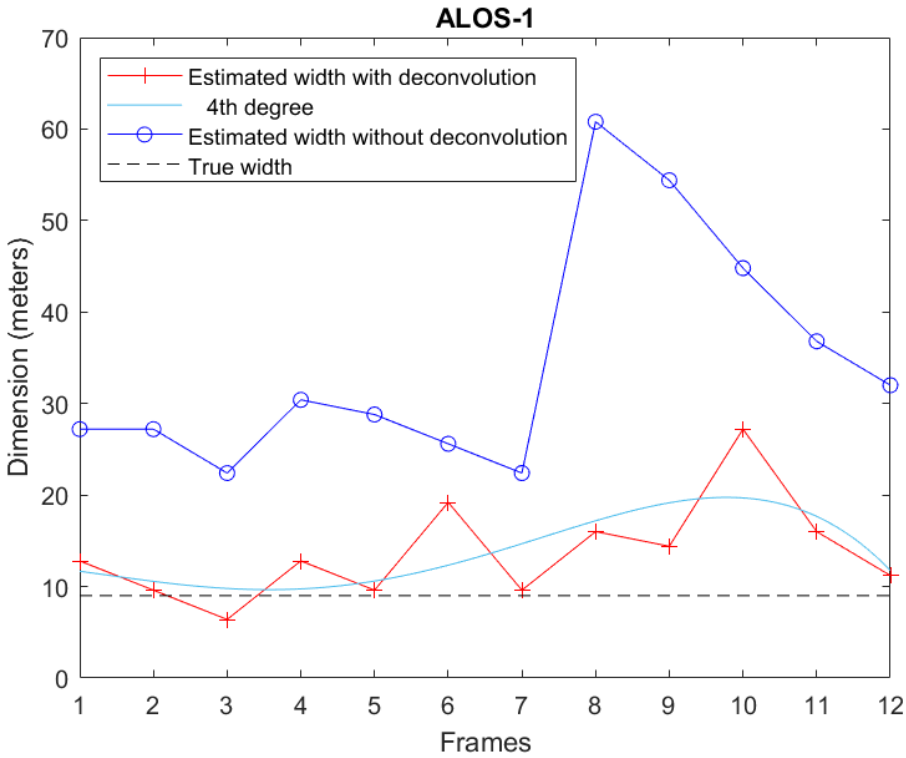

Fig.6: The estimated width of raw and deblurred images of ALOS.

3.2 SEASAT

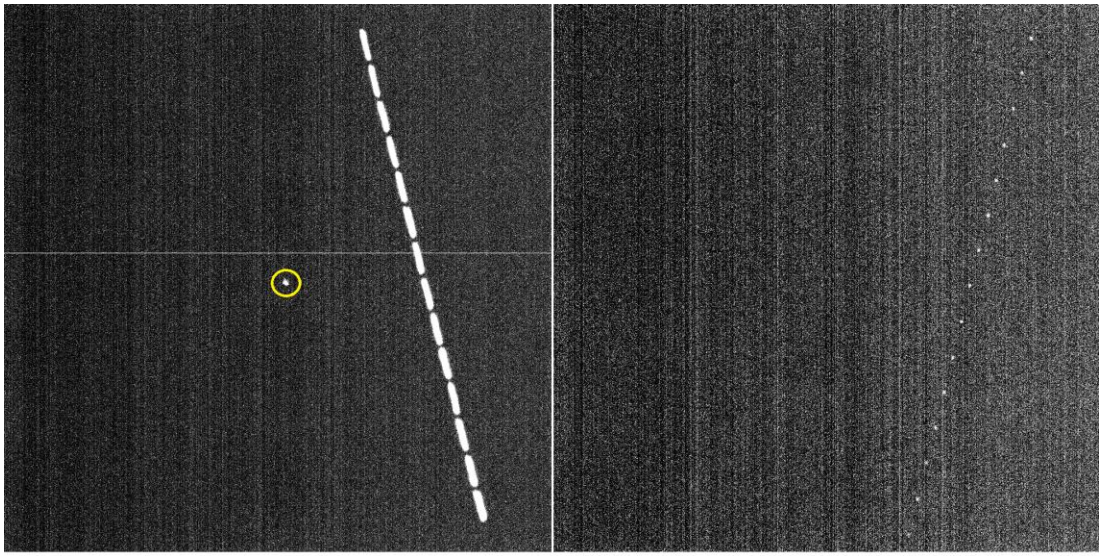

Fig.7: (a) Stacked long exposure images of SEASAT and star (HIP116653), (b) Stacked short exposure images of SEASAT.

The SEASAT in Fig.7 was imaged on 1st November 2020. During the observation, the visible magnitude of SEASAT is 2.8, elevation was 56 degrees, slanting distance (R) was 898 km, and required exposure time to image the satellite without motion blur is 0.35 ms, which is shown in Fig.7(b), imaged by short exposure camera. The telescope is pointed to the on-axis star (HIP116653) shown in yellow circle in Fig.7(a) imaged by the long exposure camera. The visible magnitude of the star HIP116653 is 6 and exposure time of 20 ms is used to image the star. When the satellite enters the FoV with star at the center, the trigger system is activated to capture frames in both cameras simultaneously. In total, 16 frames are captured within the FoV and 6 frames closest to the star on either side are processed.

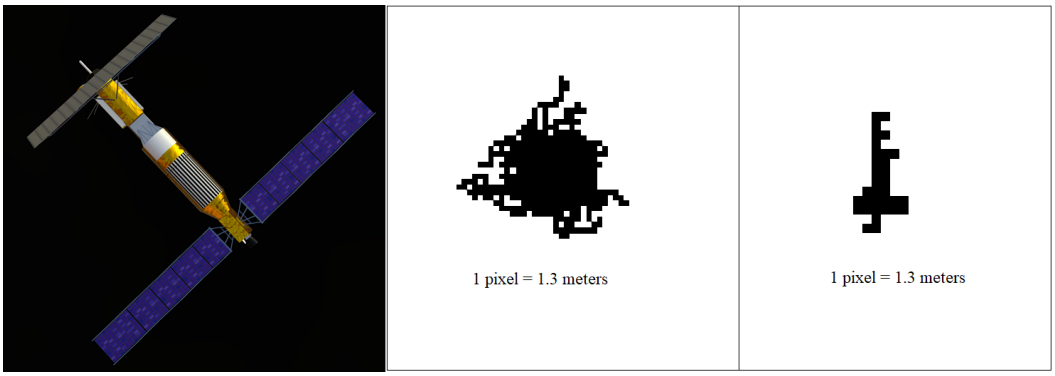

Fig.8(a), CAD model of SEASAT [9], (b) Raw image of SEASAT(7th frame), (c) Deblurred image of SEASAT (7th frame).

Fig.8(a), shows the CAD model of SEASAT, Fig.8(b) is the raw image of SEASAT without deconvolution and Fig.8(c) is the deblurred image of SEASAT after applying the Lucy-Richardson algorithm. True length and width of SEASAT is 21 and 14.5 meters respectively [9]. Fig.8 (b & c) are the short exposure image from frame 7. The local mean value (intensity) of the image is 17 (8 bit), pixels above the mean value are extracted, grouped and identified as a satellite, which is shown in Fig.8(b). The estimated length and width of the image in Fig.8(b) is 32m and 31 m respectively. The estimated length and width of the image in Fig.8(c) is 19.2 and 6.4m, which is in close proximity to true length but varies from the width of SEASAT.

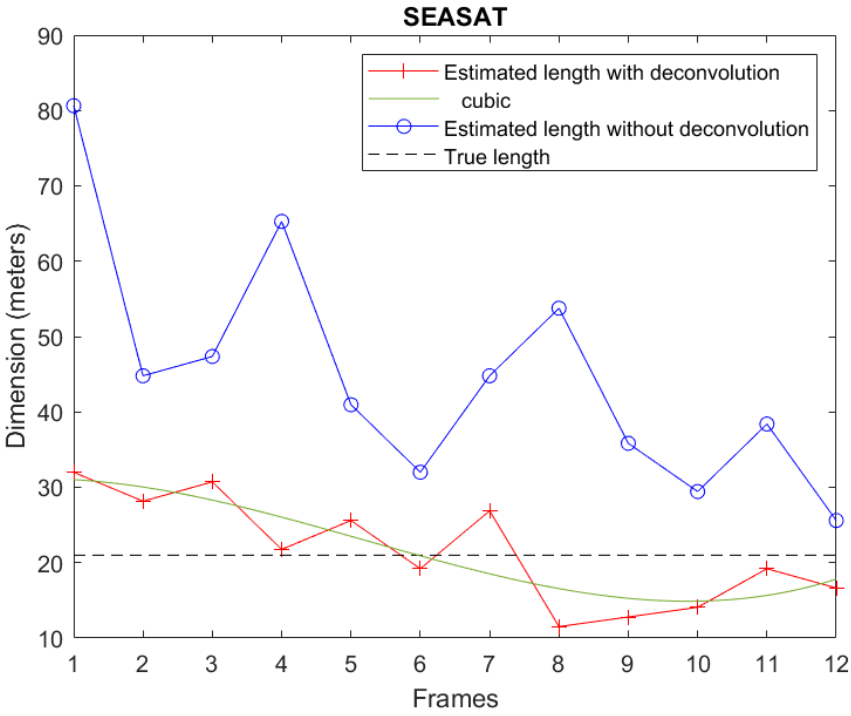

Fig.9: The estimated length of raw and deblurred images of SEASAT.

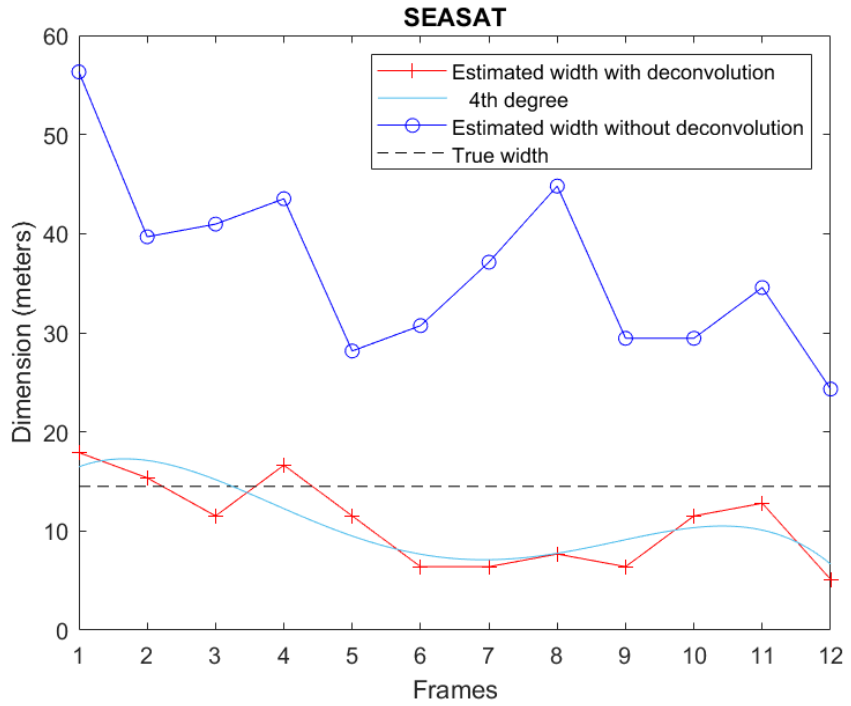

Fig.10: The estimated width of raw and deblurred images of SEASAT.

Fig.9 shows the estimated length of SEASAT with and without deconvolution. The raw image of SEASAT shown in Fig.8(b) looks like a blob and it does not reveal any physical structure of the satellite because the raw image has been blurred by atmospheric turbulence, hence the estimated length of SEASAT in raw image (without deconvolution) differs largely from the true length (21m), which is shown in Fig.9. However, after the deconvolution the blurred

image is partially restored, which is show in Fig.8(c), hence the estimated length with deconvolution in corresponds with the true length of SEASAT in Fig.9.

Six frames on either side closest to the star are processed in Fig.9. The shortest distance between the SEASAT and the reference star is 502 pixels in frame 6 and the corresponding angular distance is 150 arcseconds (2.5 arcminutes). The estimated length with deconvolution corresponds with the true length at frame 4 and 6, but varies moderately over the rest of the frames. Due to angular anisoplanatism, the trend line (cubic) in Fig.9 implies that the accuracy after deconvolution is higher when the satellite is closer to the star and the accuracy decreases when the satellite is further away from the star. Fig.10 shows the estimated width of the SEASAT with and without deconvolution. Frames 2, 4 and 11 corresponds with the true width (14.5 m) but the rest of the frames vary moderately from the true width.

4. CONCLUSION

A new technique has been detailed to deblur satellite images in LEO and this method implements a multi-exposure time (dual camera system) to image both a closely separated background star and the satellite in a FoV. The estimated length of the satellite (ALOS & SEASAT) after deconvolution coincides with the true length of the satellites. The trend line of estimated length with deconvolution shows that due to angular anisoplanatism the quality of deconvolution (Lucy-Richardson algorithm) increases as the satellite is closer to the star in the center of FoV. However, when compared to the estimated length, the accuracy of the estimated width is lower due to error in estimating the minor axis of the satellite. Hence, a customized algorithm is required to process the minor axis of the satellite. This proposed method is cost effective and less computationally expensive when compared to the conventional real time correction system. The ability to resolve smaller and fainter satellites (Mv >3) with high accuracy and SNR can be achieved by using the 1 meter telescope at UCMJO in future.

ACKNOWLEDGMENTS

The authors would like to acknowledge and thank the staff at University of Canterbury Mt. John Observatory. This research was supported by the Marsden Fund Contract (MFP UOC1803), administered by the Royal Society of New Zealand.

REFERENCES

[1] VA Muruganandan, A Lambert, R Clare, S Weddell, “Spatial Characteristics of Functional and Non-functional Satellites in Low Earth Orbit”, 8th European conference on space debris, Germany, 2021.

[2] WH Richardson, “Bayesian-based iterative method of image restoration” JoSA, vol. 62, no. 1, pp. 55–59, 1972.

[3] S Hickman, VA Muruganandan, R Clare, S Weddell, “Image metrics for Deconvolution of Satellites in Low Earth Orbit” *IEEE* 978-1-7281-8579, 2020.

[4] EO portal directory. (2022) About ALOS. [online] https://earth.esa.int/web/eoportal/satellite-missions/a/alos

[5] EO portal directory. (2022) About SEASAT. [online] https://earth.esa.int/web/eoportal/satellite-missions/s/seasat

[6] Matlab Version 9.6.0.1335978 (R2019a) Update 8, The Mathworks, Inc., Natick, Massachusetts.

[7] S Weddell, “Optical Wavefront Prediction with Reservoir Computing” PhD thesis, University of Canterbury, 2010.

[8] 3D Warehouse. (2021) ALOS (3d model). [online] Available: https://3dwarehouse.sketchup.com/search/?q=advanced%20land%20observing%20satellite%2 0daichi%20alos&searchTab=model

[9] Sketchfab. (2021) SEASAT (3d model). [online] Available: https://sketchfab.com/3d-models/seasat-05acd7198d60421eb9b9c6ed194d9166